Evolution of fission-fragment mass distributions in the neutron-deficient lead region

L. Ghys *et al.*

Phys. Rev. C **90**, 041301 — Published 15 October 2014
DOI: 10.1103/PhysRevC.90.041301

The Evolution of Fission-Fragment Mass Distributions in the Neutron-Deficient Lead Region

L. Ghys,[1,2,*] A.N. Andreyev,[3,4,5] M. Huyse,[1] P. Van Duppen,[1] S. Sels,[1] B. Andel,[6] S. Antalic,[6] A. Barzakh,[7] L. Capponi,[5] T.E. Cocolios,[8,9] X. Derkx,[5,10] H. De Witte,[1] J. Elseviers,[1] D.V. Fedorov,[7] V.N. Fedosseev,[11] F.P. Hessberger,[12,13] Z. Kalaninová,[6] U. Köster,[14] J.F.W. Lane,[5] V. Liberati,[5] K.M. Lynch,[9,8] B.A. Marsh,[11] S. Mitsuoka,[4] P. Möller,[15] Y. Nagame,[4] K. Nishio,[4] S. Ota,[4] D. Pauwels,[2] R.D. Page,[16] L. Popescu,[2] D. Radulov,[1] M.M. Rajabali,[1] J. Randrup,[17] E. Rapisarda,[8] S. Rothe,[11,18] K. Sandhu,[5] M.D. Seliverstov,[3,7,5,1] A.M. Sjödin,[11] V.L. Truesdale,[3] C. Van Beveren,[1] P. Van den Bergh,[1] Y. Wakabayashi,[4,19] and M. Warda[20]

[1] *KU Leuven, Instituut voor Kern- en Stralingsfysica, 3001 Leuven, Belgium*
[2] *Belgian Nuclear Research Center SCK•CEN, Boeretang 200, B-2400 Mol, Belgium*
[3] *Department of Physics, University of York, York, YO10 5DD, United Kingdom*
[4] *Advanced Science Research Center, Japan Atomic Energy Agency, Tokai-Mura, Naka-gun, Ibaraki, 319-1195, Japan*
[5] *School of Engineering, University of the West of Scotland, Paisley, PA1 2BE, United Kingdom*
[6] *Departement of Nuclear Physics and Biophysics, Comenius University, 84248 Bratislava, Slovakia*
[7] *Petersburg Nuclear Physics Institute, NRC Kurchatov Institute, Gatchina 188300, Russia*
[8] *PH Departement, CERN, CH-1211 Geneve 23, Switzerland*
[9] *School of Physics and Astronomy, The University of Manchester, M13 9PL, United Kingdom*
[10] *LPC, ENSICAEN, Universit de Caen Basse Normandie, CNRS/IN2P3-ENSI, F-14050, France*
[11] *EN Departement, CERN, CH-1211 Geneve 23, Switzerland*
[12] *Gesellschaft für Schwerionenforschung, Planckstrasse 1, D-64291 Darmstadt, Germany*
[13] *Helmholtz Institut Mainz, 55099 Mainz, Germany*
[14] *Institut Laue Langevin, 71 avenue des Martyrs, F-38042 Grenoble Cedex 9, France*
[15] *Theoretical Division, Los Alamos National Laboratory, Los Alamos, New Mexico 87545, USA*
[16] *Departement of Physics, Oliver Lodge Laboratory, University of Liverpool, Liverpool L69 7ZE, United Kingdom*
[17] *Nuclear Science Division, Lawrence Berkeley National Laboratory, Berkeley, California 94720, USA*
[18] *Institut für Physik, Johannes Gutenberg-Universität Mainz, D-55128 Mainz, Germany*
[19] *RIKEN Nishina Center for Accelerator Based Science, Wako, Saitama 351 0198, Japan*
[20] *Institute of Physics, Marie Curie-Sklodowska University, pl. M. Curie-Sklodowskiej 1, 20-031 Lublin, Poland*
(Dated: Received: September 23, 2014)

Low-energy β-delayed fission of ^{194,196}At and ^{200,202}Fr was studied in detail at the mass separator ISOLDE at CERN. The fission-fragment mass distributions of daughter nuclei ^{194,196}Po and ^{202}Rn indicate a triple-humped structure, marking the transition between asymmetric fission of ^{178,180}Hg and symmetric fission in the light Ra-Rn nuclei. Comparison with the macroscopic-microscopic finite-range liquid-drop model and the self-consistent approach employing the Gogny D1S energy density functional yields discrepancies. This demonstrates once more the need of dynamical fission calculations, as for both models the potential-energy surfaces lack pronounced structures, in contrast to the actinide region.

Nuclear fission, the division of a heavy atomic nucleus into predominantly two parts, continues to provide new and unexpected features in spite of a long history of intensive theoretical and experimental studies [1–7]. The fission process is not only important for several applications, such as energy production and radiopharmacology, but also has a direct impact on the understanding of the fission recycling process in r-process nucleosynthesis [8, 9]. Therefore, a description of the fission process with reliable predictive power is needed, in particular for low-energy fission where the fission-fragment (FF) mass distributions are strongly sensitive to microscopic effects [4]. Mass distributions (MDs) are usually predominantly symmetric or asymmetric with the yields exhibiting a single peak or two distinct peaks, respectively. However, in several cases a mixture of two modes was observed [5]. Experimental observables characterizing various fission modes are the width of the MD peak(s), the position of these peaks in asymmetric mass division and total kinetic energy (TKE) of the FFs.

The dominance of asymmetric fission in most of the actinide region beyond A = 226 up to about ^{256}Fm was attributed to strong microscopic effects of the heavier FF, near the doubly-magic ^{132}Sn [4, 10, 11]. However, nuclei such as ^{258}Fm and ^{259,260}Md exhibit complex MDs, each with a narrow and a broad symmetric component with a higher and lower TKE, respectively.

* lars.ghys@fys.kuleuven.be

This phenomenon is called bimodal fission [12–15]. Competition between symmetric and asymmetric fission, corresponding to respectively lower and higher TKE and resulting in a triple-humped MD has been reported around ^{226}Th [16–18]. These observations strongly support the hypothesis that nuclei may fission through several independent fission modes corresponding to different pre-scission shapes and fission paths in a multidimensional potential-energy landscape, referred to in literature as multimodal or multichannel fission [4, 5, 11, 16–19].

In the pre-actinide region, predominantly symmetric FF mass distributions were measured. A few relevant cases for the present discussion (see also Fig.1) are ^{195}Au, ^{198}Hg and ^{208,210}Po, studied by means of charged-particle induced reactions [20–22] and ^{204,206,208}Rn studied via electromagnetically (EM)-induced fission [23, 24].

In contrast to this, recent β-delayed fission experiments have established a new region of asymmetry around nuclei ^{178,180}Hg [25–27], which in fission divide into neutron-deficient fragments with most probable mass numbers around $A_{\mathrm{L}} \sim 80$ and $A_{\mathrm{H}} \sim 100$. The mechanism behind the asymmetric MD is different from that in the uranium region, since strong shell effects in the respective FFs are absent in the neutron-deficient lead region. Several theoretical models reproduced this observation [28–31].

Extensive calculations of the FF mass yields by use of the recently developed Brownian Metropolis shape-motion treatment [32] are shown in Fig. 1. These calculations reproduced well the observed mass asymmetry of ^{178,180}Hg and symmetry of ^{204,206,208}Rn and predict a smooth transition in between. We report in this paper on the fission properties of neutron-deficient isotopes ^{194,196}Po and ^{202}Rn situated between these two regions, which were measured through the βDF process.

In this two-step process a precursor nuclide undergoes β decay to excited states near the top of the fission barrier in the daughter nucleus, which then may fission. The excitation energy of the fissionning daughter is limited by the Q_{β} value, thus typically in the region between 3 to 11 MeV. Presently, 26 βDF cases are known in the region between thallium and mendelevium [6]. Prior to this work, βDF of ^{196}At was experimentally observed in Dubna [34, 35]. In addition, recent experiments at SHIP have identified βDF of ^{192,194}At [36]. However, due to the detection methods employed, FF mass distributions remained undetermined in all three cases.

In this letter, we report on the first identification of βDF in ^{200,202}Fr and on dedicated measurements of ^{194,196}At, situated in a region where fission has scarcely been studied before. Calculations in Fig. 1 show predominantly asymmetric fission with a gradually decreasing mass split when moving from ^{178,180}Hg towards ^{204,206}Rn nuclei. In contrast to these theoretical predictions, the new results indicate complex multimodal fission of ^{194,196}Po.

The measurements were carried out in ISOLDE (CERN) [37], where astatine and francium isotopes are formed in spallation reactions via the bombardment of a 50 g/cm^2 thick UC$_x$ target by 1.4 GeV protons. Surface ionization of francium or laser-ionization of astatine [38] in the ion source of ISOLDE are employed for the respective element selection. After extraction, acceleration to 30 keV and mass separation the isotopically-purified beam is transported to the 'Windmill' detection setup, described in detail in [25, 27, 39]. There, the ion beam is implanted into one of ten 20 μg/cm^2 thick carbon foils, which are mounted on a rotatable wheel. FFs, as well as α particles, are recorded by two silicon detectors of 300 μm thickness, further denoted by Si1 and Si2, placed on either side of the foil. The detection efficiency for single FFs is ~ 51 %, while double-fold FFs are recorded with ~ 21 % efficiency [27]. After ~ 40 s, the irradiated foil is turned between another pair of silicon detectors, where longer-living daughter activity can be detected. Meanwhile, implantation and measurements continue on a fresh foil. A high-purity germanium detector was installed in close vicinity to the implantation point for γ detection (see Fig. 1 from [25]).

The experimental campaign consisted of two parts, a summary of acquired statistics is given in Table I. The first part, carried out at the High-Resolution Separator (HRS) in 2011, was mainly dedicated to βDF of ^{202}Fr. Daughter activities and the thallium isobaric beam contaminant, produced by surface ionization, were observed in the α or γ spectra respectively. Because of a low Q_{EC} value (Tl) [40] and high fission barrier (Hg) [33], βDF is severely hindered for ^{202}Tl [6]. The observed FFs are thus uniquely ascribed to the βDF of ^{202}Fr. A similar reasoning applies for the βDF measurements of ^{194,196}At and ^{200}Fr.

The data for ^{194,196}At and ^{200}Fr were mainly acquired at the General Purpose Separator (GPS) in 2012, although a limited number of βDF events for these nuclei was observed at the HRS, see Table I. The full energy spectrum after 35 hours of data collection on ^{196}At at the GPS is shown in Fig. 2. Electrons/ positrons, α particles and fission fragments ($30-90$ MeV energy) are marked in the spectrum.

The technique described in [27] allowed to deduce a βDF probability of $P_{\beta\mathrm{DF}} = 9(1) \times 10^{-5}$ for ^{196}At and a lower limit at $P_{\beta\mathrm{DF}} > 3.1(17) \times 10^{-2}$ for ^{200}Fr (in agreement with [41], where only a single event was observed). A detailed discussion on the α decay of ^{196}At is given in a forthcoming paper [42]. In the cases of ^{194}At and ^{202}Fr, $P_{\beta\mathrm{DF}}$ remains undetermined at this stage since two states (the ground state and an isomer) with unknown β branching ratios and similar half-lives are known [36, 43, 44]. Although the excitation energy of the isomeric states are most likely less then a few hundreds keV, their difference in spin and parity with respect to the ground state may result in dissimilar βDF properties. These intriguing cases will be further studied at the RILIS [45] or CRIS [46, 47] setup at

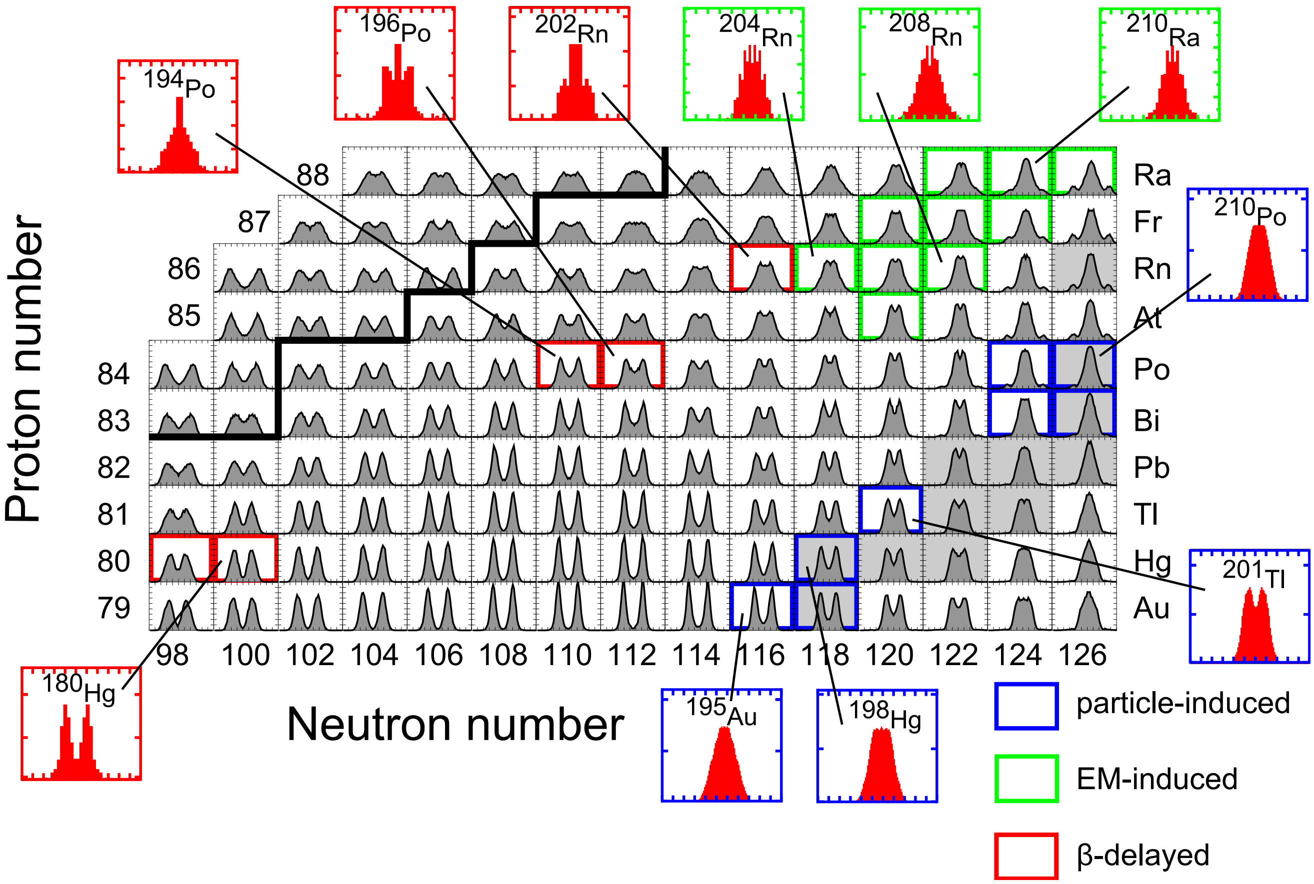

FIG. 1. (color online) Calculated MDs (gray), with fission-fragment masses on the horizontal and their relative yields on the vertical axis, for even-N neutron-deficient isotopes between gold and radium at excitation energies slightly above the theoretical fission-barrier heights $B_{\mathrm{f,th}}$ [33]. The calculated yields are compared with selected experimental MDs (red) from particle-induced [20, 21], β-delayed ([25, 26], this work) and EM-induced fission [23, 24]. The border of the lightest known isotopes is shown by the thick solid line, β-stable nuclei are shown on a gray background.

TABLE I. Summary of βDF runs giving the total number of detected single ('S') and double-fold ('D') FFs, the ratio of α to βDF decays recorded in the same detector, corrected for the detection-efficiency difference between α particles and double-fold fission events, and the total measurement time.

data set	S FFs	D FFs	$N_\alpha/N_{\beta\mathrm{df}}$	time
^{194}At - HRS	8	3	$2.0^{+17}_{-8}\times 10^3$	1h 13m
^{194}At - GPS	385	106	$1.7(1)\times 10^3$	9h 11m
^{196}At - HRS	14	5	$3.9^{+19}_{-12}\times 10^5$	5h 25m
^{196}At - GPS	273	68	$4.3(5)\times 10^5$	35h 7m
^{200}Fr - HRS	1	0	$2.5^{+123}_{-17}\times 10^3$	21h 34m
^{200}Fr - GPS	7	2	$1.5^{+12}_{-6}\times 10^3$	20h 18m
^{202}Fr - HRS	115	43	$1.4(2)\times 10^4$	43h 59m

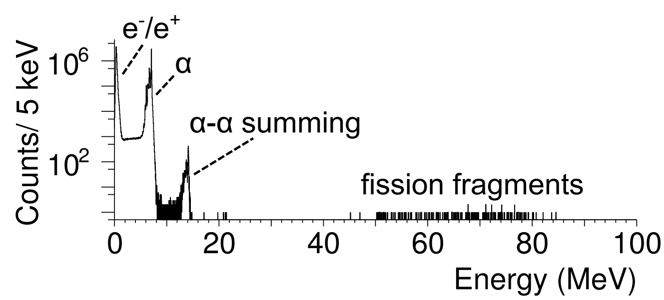

FIG. 2. The full-range energy spectrum for ^{196}At taken in the measurements at the GPS.

ISOLDE, where the production of each state might be selectively enhanced by exploiting differences in the atomic hyperfine structure.

The Si detectors were individually calibrated with mass- and energy-separated beams at the FF separator LOHENGRIN at ILL, enabling a precise conversion of the measured energy distributions in MDs [27]. A possible emission of prompt neutrons would cause a shift in TKE of about 0.7 MeV per emitted neutron [27]. However, total energy-balance considerations limit the number of prompt neutrons to a maximum of two per fission event in studied nuclei. Since this emission can only marginally influence MDs, the corresponding energy correction was neglected.

The resulting mass and energy distributions of coincident FFs after βDF of ^{194,196}At and ^{202}Fr are shown in Fig. 3 including, as a reference, the data from ^{180}Tl [27]. Because of low statistics, ^{200}Fr is excluded. For ^{180}Tl, asymmetric fission was clearly observed as a double-humped structure in the two-dimensional Si1-Si2 energy plot at the top, showing the energies of two coincident fission fragments. The single Gaussian-like TKE distribution, depicted in the middle row, indicates that for the βDF of ^{180}Tl one fission mode dominates. Finally, the deduced clearly asymmetric MD is depicted in black at the bottom.
In contrast to ^{180}Tl, a single broad hump is seen in the 2D energy distribution for the βDF of ^{194,196}At and ^{202}Fr. In addition, TKE distributions are significantly broader compared to the ^{180}Tl reference as can be concluded from the standard deviation values, extracted from single Gaussian fits, see Table II. Mass spectra, drawn in black, exhibit a mixture of symmetry with asymmetry.
The indication of triple-humped MDs and breadth of the extracted TKE suggest the presence of at least two distinct fission modes each having different mass and TKE distributions. This feature was therefore further investigated by discriminating between fission events with high or low TKE, similar to the method described in [12, 13] used to illustrate bimodal fission in the transfermium region.
In Fig. 3, MDs of fission events with respectively higher or lower TKE in comparison to a certain threshold energy E_{thres} are shown by respectively the dashed blue and full green line. The value E_{thres} was arbitrarily taken as the mean TKE value listed in Table II and is indicated by a dashed red line on the TKE distributions and the 2-D energy plots. Remarkably, the ^{194,196}At cases exhibit a narrow symmetric distribution for fragments with higher TKE, while a broader, possibly asymmetric structure is observed for lower TKE. In contrast, this feature is absent in the βDF of ^{180}Tl, in which only one asymmetric fission mode was identified. In the case of ^{202}Fr, statistics prohibit drawing definitive conclusions.
The asymmetry was quantified in Table II as $\Delta A/A_{\mathrm{tot}}$, where A_{tot} represents the compound-nucleus mass and ΔA the difference between the most probable mass numbers of the observed heavy and light asymmetric FFs, obtained from Gaussian fits to the total mass spectra.

The data have been compared with two theoretical descriptions. The microscopic HFB theory with Gogny D1S nuclear force [29, 48, 49], see Fig. 4, shows a broad and flat plateau in the potential-energy surface (PES) with numerous weakly-pronounced valleys and ridges, not exceeding 2 MeV energy difference, for a wide range of quadrupole (beyond $Q_2 = 100$ b) and octupole deformations. Such a pattern in the PES for ^{196}Po, without well-defined fission valleys, leads to a variety of fission paths possibly giving rise to a mixture of symmetric and asymmetric MD. Ignoring thermal fluctuations, three fission paths with different scission-point shapes can be identified (see inset in Fig. 4): one symmetric (A), one with almost symmetric FF masses (C) and one asymmetric (B). Within the current model, the full FF mass distribution as well as the balance between various modes remains however undetermined. Furthermore, in contrast to the actinides where clear valleys in the PES that lead to fission are present, the rather flat PES plateau in this region necessitates the inclusion of dynamic effects in describing the fission process.
The finite-range liquid-drop model (FRLDM) calculations, which show similar PES patterns as compared to the HFB calculations for nuclei in this region [28], were combined with the Brownian shape-motion model in order to calculate FF mass distributions [50, 51]. As shown in Fig. 1 and further discussed in [52], there is reasonable agreement between the calculations and most of the experimental data earlier obtained. Also the experimental triple-humped MDs in the transition region between symmetry and asymmetry around ^{226}Th, resulting from a competition between symmetric and asymmetric fission channels, were reproduced with fair accuracy [32, 50]. However, the FRLDM calculations show only one asymmetric fission channel, with a gradual decrease of the mass split, during the transition from distinctly asymmetric in ^{178,180}Hg towards symmetry in the Ra-Rn nuclei. This is in contrast to the experimental findings that show a different mass distribution (see Fig. 3) and a constant relative mass split of the asymmetric component between ^{180}Hg and ^{202}Rn (see Table II).

In conclusion, our experimental data for ^{194,196}Po and ^{202}Rn suggest a new region of multimodal fission in the neutron-deficient lead region. Calculations based on modern approaches (FRLDM and HFB) show broad and flat potential-energy surfaces in this region, making

TABLE II. Characteristic parameters of TKE and mass distributions shown in Fig. 3, when assuming no prompt neutrons are emitted. The mean value $\overline{\mathrm{TKE}}$, standard deviation σ of the respective Gaussian fits are given, as well as corresponding statistical errors. In addition, the lower mass number A_{L} and the relative mass split $\Delta A/A_{\mathrm{tot}}$ of asymmetric fission are listed.

	$\overline{\mathrm{TKE}}$ (MeV)	σ (MeV)	A_{L}	$\Delta A/A_{\mathrm{tot}}$
$^{180}\mathrm{Tl} \xrightarrow{\beta} {}^{180}\mathrm{Hg}$ (ff) [a]	133.1(3)	6.1(3)	80(1)	0.11(1)
$^{194}\mathrm{At} \xrightarrow{\beta} {}^{194}\mathrm{Po}$ (ff)	146(1)	9.0(13)	-	-
$^{196}\mathrm{At} \xrightarrow{\beta} {}^{196}\mathrm{Po}$ (ff)	147(1)	8.1(15)	88(2)	0.10(2)
$^{202}\mathrm{Fr} \xrightarrow{\beta} {}^{202}\mathrm{Rn}$ (ff)	149(2)	10(3)	89(2)	0.12(2)

[a] data taken from [27]

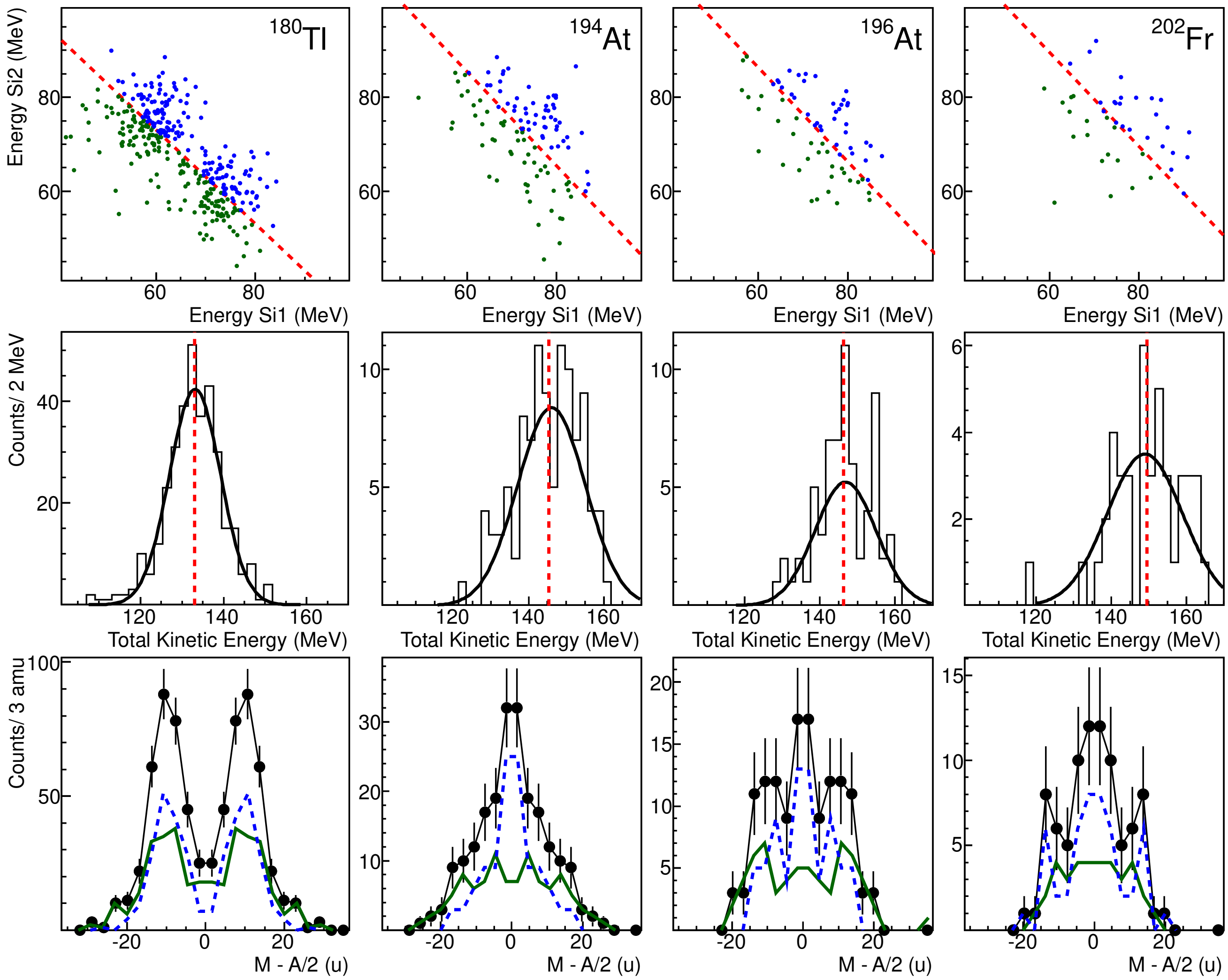

FIG. 3. (color online) Summary plot of the 2D energy distribution of coincident FFs in 2 silicon detectors (top), total kinetic energy (middle) and mass distributions (bottom) of investigated nuclei. The green and blue curves represent data below and above the average TKE given in Table II. Details are given in the main text.

it difficult to identify unique fission paths but providing a much better testing ground for the dynamical description of fission, as compared to the actinide region where strong structures in the PES determine the MDs. In addition, the ground and isomeric states in ^{194}At and ^{202}Fr may exhibit different βDF behaviors, both in terms of FF mass distributions and β-delayed fission probabilities. These cases provide a unique experimental way to study the spin and parity dependence of fission and will therefore be further investigated at ISOLDE-CERN using selective laser-ionization techniques [45, 46].

Acknowledgements. We thank the ISOLDE collaboration for providing excellent beams and the GSI Target Group for manufacturing the carbon foils. Also, we express our gratitude to K.-H. Schmidt for providing the files containing measured fission-fragment element distributions in EM-induced fission, shown in Fig. 1. A part of this work was done during the Program INT-13-3 ‘Quantitative Large Amplitude Shape Dynamics: Fission and heavy ion fusion’ at the National Institute for Nuclear Theory in Seattle. This work has been funded by FWO-Vlaanderen (Belgium), by GOA/2010/010 (BOF KU Leuven), by the Interuniversity Attraction Poles Programme initiated by the Belgian Science Policy Office (BriX network P7/12), by the European Commission within the Seventh Framework Programme through I3-ENSAR (contract no. RII3-CT-2010-262010), by a grant from the European Research Council (ERC-2011-AdG-291561-HELIOS), by the Slovak Research and Development Agency (Contract No. APVV-0105-10), by the Office of Nuclear Physics in the U.S. Department of Energy’s Office of Science under Contract No. DE-AC02-05CH11231, by the National Nuclear Security Administration of the U.S. Department of Energy at Los Alamos National Laboratory under Contract No. DE-

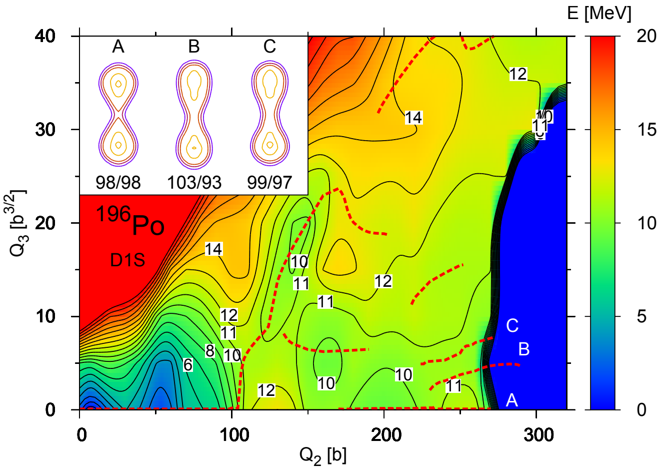

FIG. 4. (in color) Calculated PES for ^{196}Po from a microscopic HFB theory [29, 48, 49]. Lines of constant energy are plotted every 1 MeV. Dashed lines represent fission paths. Scission-point shapes and corresponding mass ratios for three fission paths A-C are shown in the inset.

AC52-06NA25396, by the UK Science and Technology Facilities Council (STFC) and by the Reimei Foundation of JAEA.

[1] O. Hahn and F. Strassmann, Naturwissenschaften **27**, 11 (1939).

[2] L. Meitner and O. R. Frisch, Nature **143**, 239 (1939).

[3] H. L. Hall and D. C. Hoffman, J. Radioanal. Nucl. Chem. **142**, 53 (1990).

[4] C. Wagemans, *The nuclear fission process*, edited by C. Wagemans (1991).

[5] Y. Nagame and H. Nakahara, Radiochim. Acta **100**, 605 (2012).

[6] A. N. Andreyev, M. Huyse, and P. Van Duppen, Rev. Mod. Phys. **85**, 1541 (2013).

[7] M. Bender, P.-H. Heenen, and P.-G. Reinhard, Rev. Mod. Phys. **75**, 121 (2003).

[8] I. V. Panov, E. Kolbe, B. Pfeiffer, T. Rauscher, K.-L. Kratz, and F.-K. Thielemann, Nucl. Phys. A **747**, 633 (2005).

[9] I. Petermann, K. Langanke, G. Martínez-Pinedo, I. V. Panov, P. G. Reinhard, and F. K. Thielemann, Eur. Phys. J. A **48**, 122 (2012).

[10] J. F. Berger, M. Girod, and D. Gogny, Nucl. Phys. A **428**, 23c (1984).

[11] P. Möller, D. G. Madland, A. J. Sierk, and A. Iwamoto, Nature **409**, 785 (2001).

[12] E. K. Hulet, J. F. Wild, R. J. Dougan, R. W. Lougheed, J. H. Landrum, A. D. Dougan, M. Schädel, R. L. Hahn, P. A. Baisden, C. M. Henderson, R. J. Dupzyk, K. Sümmerer, and G. R. Bethune, Phys. Rev. Lett. **56**, 313 (1986).

[13] E. K. Hulet, J. F. Wild, R. J. Dougan, R. W. Lougheed, J. H. Landrum, A. D. Dougan, P. A. Baisden, C. M. Henderson, R. J. Dupzyk, R. L. Hahn, M. Schädel, K. Sümmerer, and G. R. Bethune, Phys. Rev. C **40**, 770 (1989).

[14] P. Möller, J. R. Nix, and W. J. Swiatecki, Nucl. Phys. A **469**, 1 (1987).

[15] S. Ćwiok, P. Rozmej, A. Sobiczewski, and Z. Patyk, Nucl. Phys. A **491**, 281 (1989).

[16] H. C. Britt, H. E. Wegner, and J. C. Gursky, Phys. Rev. **129**, 2239 (1963).

[17] E. Konecny and H. W. Schmitt, Phys. Rev. **172**, 1213 (1968).

[18] E. Konecny, H. J. Specht, and J. Weber, in *Third IAEA Symp. Phys. Chem. Fission* (1974) pp. 3–18.

[19] U. Brosa, S. Grossmann, and A. Müller, Phys. Rep. **197**, 167 (1990).

[20] M. G. Itkis, V. N. Okolovich, and G. N. Smirenkin, Nucl. Phys. A **502**, 243c (1989).

[21] M. G. Itkis, N. A. Kondrat'ev, S. I. Mul'gin, V. N. Okolovich, Y. A. Rusanov, and G. N. Smirenkin, Sov. J. Nucl. Phys. **52**, 601 (1990).

[22] M. G. Itkis, N. A. Kondrat'ev, and S. I. Mul'gin, Sov. J. Nucl. Phys. **53**, 757 (1991).

[23] K.-H. Schmidt, S. Steinhäuser, C. Böckstiegel, A. Grewe, A. Heinz, A. R. Junghans, J. Benlliure, H. G. Clerc, M. de Jong, J. Müller, M. Pfützner, and B. Voss, Nucl. Phys. A **665**, 221 (2000).

[24] K.-H. Schmidt, J. Benlliure, and A. R. Junghans, Nucl. Phys. A **693**, 169 (2001).

[25] A. N. Andreyev, J. Elseviers, M. Huyse, P. Van Duppen, S. Antalic, A. Barzakh, N. Bree, T. E. Cocolios, V. F. Comas, J. Diriken, D. Fedorov, V. N. Fedosseev, S. Franchoo, J. A. Heredia, O. Ivanov, U. Köster, B. A. Marsh, K. Nishio, R. D. Page, N. Patronis, M. Seliverstov, I. Tsekhanovich, P. Van den Bergh, J. Van De Walle, M. Venhart, S. Vermote, M. Veselsky, C. Wagemans, T. Ichikawa, A. Iwamoto, P. Möller, and A. J. Sierk, Phys. Rev. Lett. **105**, 252502 (2010).

[26] V. Liberati, A. N. Andreyev, S. Antalic, A. Barzakh, T. E. Cocolios, J. Elseviers, D. Fedorov, V. N. Fedoseeev, M. Huyse, D. T. Joss, Z. Kalaninová, U. Köster, J. F. W. Lane, B. Marsh, D. Mengoni, P. Molkanov, K. Nishio, R. D. Page, N. Patronis, D. Pauwels, D. Radulov, M. Se-

liverstov, M. Sjödin, I. Tsekhanovich, P. Van den Bergh, P. Van Duppen, M. Venhart, and M. Veselský, Phys. Rev. C **88**, 044322 (2013).

[27] J. Elseviers, A. N. Andreyev, M. Huyse, P. Van Duppen, S. Antalic, A. Barzakh, N. Bree, T. E. Cocolios, V. F. Comas, J. Diriken, D. Fedorov, V. N. Fedosseev, S. Franchoo, L. Ghys, J. A. Heredia, O. Ivanov, U. Köster, B. A. Marsh, K. Nishio, R. D. Page, N. Patronis, M. D. Seliverstov, I. Tsekhanovich, P. Van den Bergh, J. Van De Walle, M. Venhart, S. Vermote, M. Veselský, and C. Wagemans, Phys. Rev. C **88**, 044321 (2013).

[28] P. Möller, J. Randrup, and A. J. Sierk, Phys. Rev. C **85**, 024306 (2012).

[29] M. Warda, A. Staszczak, and W. Nazarewicz, Phys. Rev. C **86**, 024601 (2012).

[30] S. Panebianco, J.-L. Sida, H. Goutte, J.-F. Lemaître, N. Dubray, and S. Hilaire, Phys. Rev. C **86**, 064601 (2012).

[31] A. V. Andreev, G. G. Adamian, N. V. Antonenko, and A. N. Andreyev, Phys. Rev. C **88**, 047604 (2013).

[32] J. Randrup and P. Möller, Phys. Rev. C **88**, 064606 (2013).

[33] P. Möller, A. J. Sierk, T. Ichikawa, A. Iwamoto, R. Bengtsson, H. Uhrenholt, and S. Aberg, Phys. Rev. C **79**, 064304 (2009).

[34] Y. A. Lazarev, Inst. Phys. Conf. Ser. **132**, 739 (1992).

[35] A. N. Andreyev, D. D. Bogdanov, S. Saro, G. M. Ter-Akopian, M. Veselsky, and A. V. Yeremin, Phys. Lett. B **312**, 49 (1993).

[36] A. N. Andreyev, S. Antalic, D. Ackermann, L. Bianco, S. Franchoo, S. Heinz, F. P. Hessberger, S. Hofmann, M. Huyse, Z. Kalaninová, I. Kojouharov, B. Kindler, B. Lommel, R. Mann, K. Nishio, R. D. Page, J. J. Ressler, B. Streicher, S. Saro, B. Sulignano, and P. VanDuppen, Phys. Rev. C **87**, 014317 (2013).

[37] E. Kugler, Hyperfine Interact. **129**, 23 (2000).

[38] S. Rothe, A. N. Andreyev, S. Antalic, A. Borschevsky, L. Capponi, T. E. Cocolios, H. De Witte, E. Eliav, D. V. Fedorov, V. N. Fedosseev, D. A. Fink, S. Fritzsche, L. Ghys, M. Huyse, N. Imai, U. Kaldor, Y. Kudryavtsev, U. Köster, J. F. W. Lane, J. Lassen, V. Liberati, K. M. Lynch, B. A. Marsh, K. Nishio, D. Pauwels, V. Pershina, L. Popescu, T. J. Procter, D. Radulov, S. Raeder, M. M. Rajabali, E. Rapisarda, R. E. Rossel, K. Sandhu, M. D. Seliverstov, A. M. Sjödin, P. Van den Bergh, P. Van Duppen, M. Venhart, Y. Wakabayashi, and K. D. A. Wendt, Nat. Commun. **4**, 1835 (2013).

[39] M. D. Seliverstov, T. E. Cocolios, W. Dexters, A. N. Andreyev, S. Antalic, A. E. Barzakh, B. Bastin, J. Büscher, I. G. Darby, D. V. Fedorov, V. N. Fedosseev, K. T. Flanagan, S. Franchoo, G. Huber, M. Huyse, M. Keupers, U. Köster, Y. Kudryavtsev, B. A. Marsh, P. L. Molkanov, R. D. Page, A. M. Sjödin, I. Stefan, P. Van Duppen, M. Venhart, and S. G. Zemlyanoy, Phys. Rev. C **89**, 034323 (2014).

[40] M. Wang, G. Audi, A. H. Wapstra, F. G. Kondev, M. MacCormick, X. Xu, and B. Pfeiffer, Chinese Phys. C **36**, 1603 (2012).

[41] Z. Kalaninová, S. Antalic, A. N. Andreyev, F. P. Hessberger, D. Ackermann, B. Andel, L. Bianco, S. Hofmann, M. Huyse, B. Kindler, B. Lommel, R. Mann, R. D. Page, P. J. Sapple, J. Thomson, P. Van Duppen, and M. Venhart, Phys. Rev. C **89**, 054312 (2014).

[42] V. L. Truesdale et al. \textit{(in preparation)}, (2014).

[43] M. Huyse, P. Decrock, P. Dendooven, G. Reusen, P. Van Duppen, and J. Wauters, Phys. Rev. C **46**, 1209 (1992).

[44] A. N. Andreyev, S. Antalic, D. Ackermann, L. Bianco, S. Franchoo, S. Heinz, F. P. Hessberger, S. Hofmann, M. Huyse, I. Kojouharov, B. Kindler, B. Lommel, R. Mann, K. Nishio, R. D. Page, J. J. Ressler, P. Sapple, B. Streicher, S. Šáro, B. Sulignano, J. Thomson, P. VanDuppen, and M. Venhart, Phys. Rev. C **79**, 064320 (2009).

[45] V. N. Fedosseev, D. V. Fedorov, R. Horn, G. Huber, U. Köster, J. Lassen, V. I. Mishin, M. D. Seliverstov, L. Weissman, and K. Wendt, Nucl. Instruments Methods Phys. Res. Sect. B Beam Interact. with Mater. Atoms **204**, 353 (2003).

[46] K. T. Flanagan, K. M. Lynch, J. Billowes, M. L. Bissell, I. Budinčević, T. E. Cocolios, R. P. de Groote, S. De Schepper, V. N. Fedosseev, S. Franchoo, R. F. Garcia Ruiz, H. Heylen, B. A. Marsh, G. Neyens, T. J. Procter, R. E. Rossel, S. Rothe, I. Strashnov, H. H. Stroke, and K. D. A. Wendt, Phys. Rev. Lett. **111**, 212501 (2013).

[47] K. M. Lynch, J. Billowes, M. L. Bissell, I. Budinčević, T. E. Cocolios, R. P. De Groote, S. De Schepper, V. N. Fedosseev, K. T. Flanagan, S. Franchoo, R. F. Garcia Ruiz, H. Heylen, B. A. Marsh, G. Neyens, T. J. Procter, R. E. Rossel, S. Rothe, I. Strashnov, H. H. Stroke, and K. D. A. Wendt, Phys. Rev. X **4**, 011055 (2014).

[48] L. M. Robledo, "HFBaxial code," (2002).

[49] J. L. Egido, L. M. Robledo, and R. R. Chasman, Phys. Lett. B **393**, 13 (1997).

[50] J. Randrup and P. Möller, Phys. Rev. Lett. **106**, 132503 (2011).

[51] J. Randrup, P. Möller, and A. J. Sierk, Phys. Rev. C **84**, 034613 (2011).

[52] P. Möller and J. Randrup \textit{(in preparation)}, (2014).